PROCEEDINGS OF SPIE

SPIEDigitalLibrary.org/conference-proceedings-of-spie

Calibration and performance of the infrared array camera (IRAC)

Joseph L. Hora, Giovanni G. Fazio, Steven P. Willner, Michael L. N. Ashby, Jiasheng Huang, et al.

Joseph L. Hora, Giovanni G. Fazio, Steven P. Willner, Michael L. N. Ashby, Jiasheng Huang, S. Thomas Megeath, John R. Stauffer, Eric V. Tollestrup, Zhong Wang, William J. Glaccum, Judith L. Pipher, William J. Forrest, Craig R. McCreight, Mark E. McKelvey, William F. Hoffman, Peter Eisenhardt, Jason A. Surace, William T. Reach, Samuel Harvey Moseley, Richard G. Arendt, Kenneth P. Stewart, F. David Robinson, "Calibration and performance of the infrared array camera (IRAC)," Proc. SPIE 4131, Infrared Spaceborne Remote Sensing VIII, (16 November 2000); doi: 10.1117/12.406553

Event: International Symposium on Optical Science and Technology, 2000, San Diego, CA, United States

SPIE.

Downloaded From: https://www.spiedigitallibrary.org/conference-proceedings-of-spie on 12/4/2018 Terms of Use: https://www.spiedigitallibrary.org/terms-of-use

Calibration and performance of the Infrared Array Camera (IRAC)

Joseph L. Hora[*a], Giovanni G. Fazio[a], Steven P. Willner[a], Matthew L. N. Ashby[a], Jiasheng Huang[a], S. Tom Megeath[a], John Stauffer[a], Eric V. Tollestrup[a], Zhong Wang[a], William Glaccum[b], Judith L. Pipher[b], William J. Forrest[b], Craig R. McCreight[c], Mark McKelvey[c], William F. Hoffmann[d], Peter Eisenhardt[e], Jason A. Surace[f], William Reach[f], S. Harvey Moseley[g], Richard Arendt[g], Kenneth P. Stewart[g], F. David Robinson[g]

[a]Harvard-Smithsonian Center for Astrophysics, [b]University of Rochester, [c]NASA/Ames Research Center, [d]University of Arizona, [e]Jet Propulsion Laboratory, [f]SIRTF Science Center/Caltech, [g]NASA/Goddard Space Flight Center

ABSTRACT

The Infrared Array Camera (IRAC) is one of three focal plane instruments in the Space Infrared Telescope Facility (SIRTF). IRAC is a four-channel camera that obtains simultaneous images at 3.6, 4.5, 5.8, and 8 microns. Two adjacent 5.12×5.12 arcmin fields of view in the SIRTF focal plane are viewed by the four channels in pairs (3.6 and 5.8 microns; 4.5 and 8 microns). All four detector arrays in the camera are 256×256 pixels in size, with the two shorter wavelength channels using InSb and the two longer wavelength channels using Si:As IBC detectors. We describe here the results of the instrument functionality and calibration tests completed at Goddard Space Flight Center, and provide estimates of the in-flight sensitivity and performance of IRAC in SIRTF.

Keywords: infrared astronomy, infrared arrays, calibration, SIRTF, IRAC

1. INTRODUCTION

IRAC[1] is a four-channel camera that obtains simultaneous 5.12×5.12 arcmin images at 3.6, 4.5, 5.8, and 8 μm. The pixel size is 1.2 arcsec in all bands, and two adjacent fields of view are imaged in pairs (3.6 and 5.8 μm; 4.5 and 8.0 μm) using a dichroic beamsplitter. All four detector arrays in the camera are 256×256 pixels in size. The two short wavelength channels use InSb detector arrays and the two longer wavelength channels use Si:As IBC detectors, produced by Raytheon Infrared Operations[2,3]. The camera has an internal calibration subsystem that consists of a shutter mechanism that can close off the aperture to block external light, and calibration lamps that can illuminate the detectors through the IRAC optics to measure the system responsivity.

The IRAC instrument will address the four major scientific objectives defining the SIRTF mission. These are (1) to study the early universe, (2) to search for and study brown dwarfs and superplanets, (3) to study ultraluminous galaxies and active galactic nuclei, and (4) to discover and study protoplanetary and planetary debris disks. IRAC is a powerful survey instrument because of its high sensitivity, large field, and simultaneous four-color imaging. In addition to the major goals cited above, IRAC is a general-purpose camera that can be used for a wide variety of astronomical investigations.

In this paper we describe the calibration of the instrument and the results of the ground-based measurements and tests performed, and present an estimate of IRAC's in-flight performance.

2. CALIBRATION REQUIREMENTS AND STRATEGY

The goal of the calibration task is to characterize as precisely as possible the system output for a given input. The overall requirement for the IRAC mission is that all observations be calibrated to a relative accuracy of 2%, and that the absolute accuracy of the data set be determined to better than 10%. Meeting these goals places requirements on the accuracy to which the

[*] Correspondence: Email: jhora@cfa.harvard.edu; WWW: http://cfa-www.harvard.edu/~jhora

Infrared Spaceborne Remote Sensing VIII, Marija Strojnik, Bjørn F. Andresen, Editors,
Proceedings of SPIE Vol. 4131 (2000) © 2000 SPIE · 0277-786X/00/$15.00

Downloaded From: https://www.spiedigitallibrary.org/conference-proceedings-of-spie on 12/4/2018
Terms of Use: https://www.spiedigitallibrary.org/terms-of-use

system performance must be measured, and places limits on the system instability. The purpose of the ground-based calibration measurements is to establish that IRAC will meet its sensitivity requirements, and to provide the data necessary to accurately determine the instrument calibration during mission operations.

A self-consistent relative calibration of IRAC data will be performed in-flight using sky observations combined with transmission calibrator observations as required. The sky observations will measure the complete system responsivity, and the transmission calibrator observations will allow the relative calibration to be tracked efficiently on shorter timescales, and transferred between sky observations if necessary. The relative calibration system will be placed on an absolute scale by comparison to a single fundamental absolute celestial calibrator. There will be a set of celestial calibrators in various sky locations that will be linked to the fundamental calibrator to allow efficient frequent calibration measurements as needed.

During the In-Orbit Checkout (IOC) period, several measurements will be performed to characterize the instrument and determine the optimum operating parameters. Detector characteristics will be measured, including dark images, pixel-to-pixel gain variations, and noise levels. The rate of cosmic ray events will be measured in SIRTF's unique environment. A focus check and possible adjustment will be performed. Following focus, detailed measurements of the point spread function (PSF) will be made as a function of position in the field of view (FOV). The image distortion will be characterized by observations of an open star cluster with accurate astrometric positions. A suite of calibration stars will be observed to determine the flux calibration and establish the first standard star grid. The internal calibration sources will be calibrated to astronomical standards. Observations of different locations on the sky with different background levels will allow the determination of the full-system relative responsivity over the IRAC FOVs. These observations and calibrations will establish a baseline for tracking the performance throughout the mission.

The IOC tests will help determine the details of the calibration strategy during normal mission operations. It is expected that during normal observations, calibration tasks will be done once every twelve hours (which is the period between data downlinks). The shutter would be closed to obtain darks, and also images with the internal transmission calibrator and/or flood calibrator sources on for tracking changes in responsivity and flat field. Observations of one or more astronomical standards, and possibly some sky observations to be used for flat-field determination, will be performed. IRAC will use celestial calibrators to provide the fundamental flux calibration of IRAC observations. Observation of one or more of these flux calibrators will be obtained perhaps as often as every 6 hours. The list of calibration stars will include several flux calibrators that will observable at all times during SIRTF normal operations, as well as standards near the ecliptic equator that will be closer in sky position to objects being observed near that region of the sky.

3. CALIBRATION MEASUREMENTS

The system was characterized during a series of tests performed at GSFC[4]. The cold assembly (CA) was placed in a test dewar which included a telescope simulator, test sources, and a cryogenic blackbody. The dewar has ports in which IR transmitting windows were used in some tests using external sources.

3.1. Optical performance

Phase retrieval data were obtained during each of the cold cycles, and a set of through-focus images were taken to determine the best focus location and encircled energy (EE) for each channel. The phase retrieval analysis showed that the IRAC optics are diffraction-limited in all channels, with the RMS wavefront error ranging from $\lambda/20$ to $\lambda/40$. The EE measurements showed that at best focus, the ratio between the measured and expected EE in each channel was approximately 90%. The best focus positions for each of the channels are within ± 0.62 mm of the nominal SIRTF focus position

3.1.1. Magnification, distortion, PSF characterization

The test procedure involved moving the test point source and telescope simulator in a 5x5 grid across the FOV of each channel and taking a set of images at each location. Figure 1 shows the image of all the separate PSF measurements superposed on the array in one image. The PSF is relatively constant across the array. The input image provided by the telescope simulator is slightly elongated along the rows of the image, and this shape can be seen in the IRAC images as well. There is also a scattered light glint from the light source housing to the lower left of the main PSF. The image at the lower left used a lower source intensity, so it appears dimmer in the mosaic image. At each of the positions shown in Figure 1, a 4x4 grid of 0.25

Downloaded From: https://www.spiedigitallibrary.org/conference-proceedings-of-spie on 12/4/2018
Terms of Use: https://www.spiedigitallibrary.org/terms-of-use

pixel steps of the translation stage were done, and images taken at each position. Those images were combined using the drizzle technique[5] to create the final PSF image. However, for computing the centroids for the distortion characterization, a single image was used at each of the 5x5 grid points.

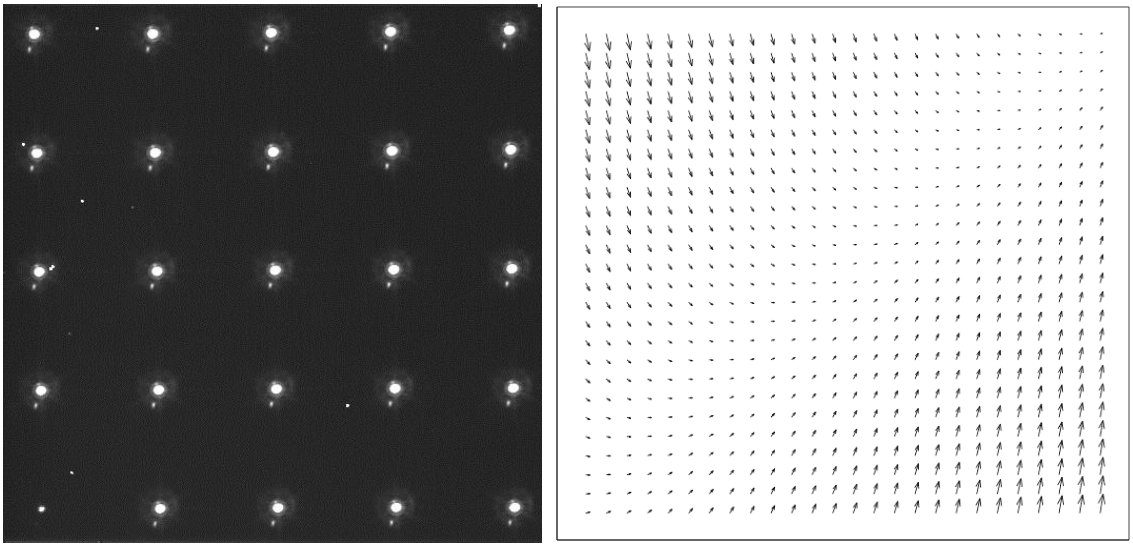

Figure 1. Channel 1 PSF and distortion. The image on the left is a mosaic of the individual PSF measurements. The image on the right shows the distortion vectors, expanded by a factor of 10 for clarity.

Also shown in Figure 1 is the distortion of the channel 1 optics relative to a rectangular grid. The maximum pixel displacement relative to the rectangular grid is approximately 1.5 pixels in X or Y. The distortion has been fit with a second order equation in X and Y with an RMS error of 0.1 pixels, which is mostly due to the measurement uncertainty in the image centroids.

3.2. Relative spectral response

The filter bandwidths and central wavelengths were calculated from the instrument transmission model. This model includes measurements of all of the IRAC components in the optical system[6], and estimates of the relative detector DQE spectral variations. The sensitivity estimate and the plot in Figure 2 used an average of the two polarization states. The plot also includes the detector QE dependence, which was measured for similar devices, and scaled to match the average QE measured for the channel. The individual component transmissions and reflections were multiplied together to obtain the instrument total optical throughput, which is defined as the average over the central 90% of the bandwidth.

3.3. Flat field

The Flat Field for each channel is taken to mean the factors by which one would have to correct each pixel to give the same value if the illumination to each pixel on the array was uniform. The factor includes the transmission of the optics, as well as the quantum efficiency of the pixel. This measurement was performed by illuminating the field of view with a cold (70-120K) blackbody source that was moved around the FOV of each channel pair. The data analyzed at GSFC by first subtracting the median of measured dark frames from the raw data (§3.5.1). Then the drifting temperature of the blackbody source and an uncorrected image of the source were iteratively determined. Finally, the flat fields were determined with a least squares fit between individual frames and the uncorrected source image. A simultaneous least-squares solution for all parameters[7] was impractical because of the drifting blackbody temperature and the regular spacing of the movements. The regular positioning of the blackbody source induces a grid-like artifact in the flat fields with a spacing ~1/4 the width of the array, especially visible in channels 3 & 4. Images of the flat fields are shown in Figure 3.

One major feature in channels 1 and 3 is a dark "shadow" on the left side of the image due to vignetting. The vignetting is present because the two channels are offset from their ideal positions. A decision was made not to correct it. However, the amplitude of the vignetting is at worst ~30% along the edge of channel 1 and ~50% in the very corner, and for channel 3 only

Downloaded From: https://www.spiedigitallibrary.org/conference-proceedings-of-spie on 12/4/2018
Terms of Use: https://www.spiedigitallibrary.org/terms-of-use

15-25% in the edge-corner areas. Approximately 12 pixel columns are below 90% in channel 1, and 6 columns below 90% in channel 3. These pixels can be corrected for in data processing, with a reduction in the sensitivity of channel 1 to 2.7 μJy in 500 seconds, which still meets our sensitivity requirement of 3 μJy for that channel.

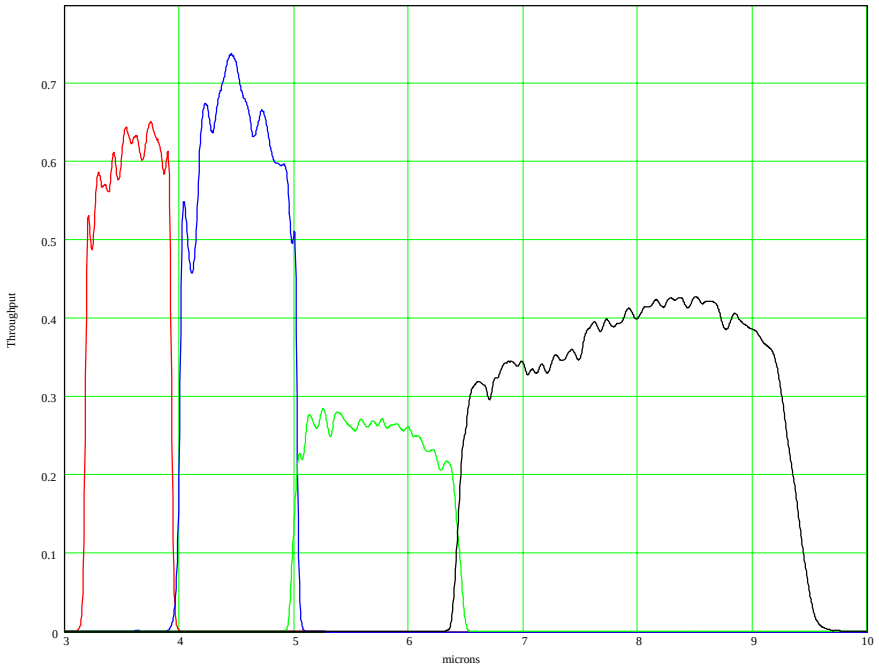

Figure 2. IRAC Total instrument throughput, e^-/photon.

The degree of vignetting deduced may also be an overestimate because of the measurement technique. The FOVs were illuminated by a blackbody source that was located in front of the pickoff mirror, not filling the full FOV. Since there were no optics external to IRAC in the beam, the defining aperture in the system was the IRAC cold stop, which is oversized by about 15% and would give an input beam larger than is going to be provided by the telescope. Therefore the vignetting in the telescope will be slightly less than seen in this configuration and will have to be calibrated by in-flight observations.

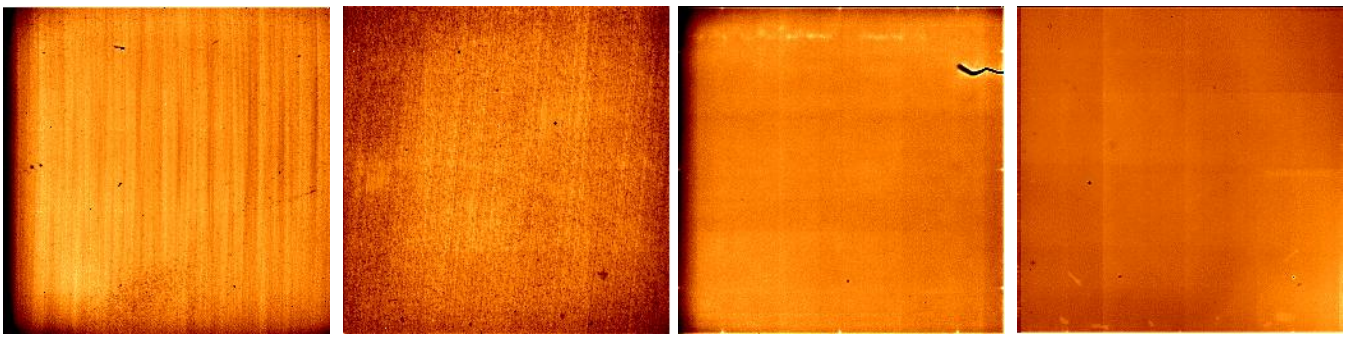

Figure 3. IRAC Flat Fields as measured with External Blackbody. L to R: Ch 1 – 4. The 1σ RMS of the images (excluding the outer 30 pixels) are 2.2%, 3.5%, 0.8%, and 0.9% for channels 1-4, respectively. The fiber in channel 3 is no longer present on the array surface.

3.4. Shutter attenuation

The attenuation of a point source in the center of the field was measured with the test point source in channel 3. The lamp was turned up to give a peak signal value of 46,000 ADU (Analog to Digital Units) in a 1 second frame time (approximately 3.7 e^-/ADU). Then the shutter was closed and a 200 sec frame taken. The expected signal in the image without the shutter

Downloaded From: https://www.spiedigitallibrary.org/conference-proceedings-of-spie on 12/4/2018
Terms of Use: https://www.spiedigitallibrary.org/terms-of-use

would be 1.13E7 ADU in the peak pixel, based on the ratio between the exposure times (many times the saturation level). The measured image level at that location was 0 ± 5 ADU, for a lower limit to the attenuation of 2.3E-6.

The attenuation of the shutter of an extended source was measured with a warm blackbody source external to the instrument whose aperture filled the field of view of IRAC. Figure 4 shows the images taken during this test in channels 2 and 4 showing the pattern of the light that is leaking around the shutter. The external illumination level and attenuation is summarized in the table below. The value for channel 1 is an upper limit.

Table 1. Shutter Attenuation

Channel	Illumination (ADU/sec)	Attenuation factor
1	7935	>1.7E-5
2	73330	2.8E-6
3	155000	3.9E-6
4	1429221	5.3E-7

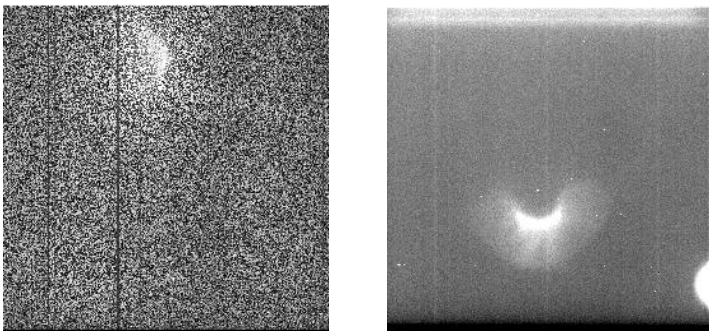

Figure 4. Channel 2 (left) and channel 4 (right) 200 second shutter attenuation images.

The appearance of channel 3 is similar to channel 4. There was no leak detected in channel 1 due to the lower blackbody flux at that wavelength. The measured performance or upper limit meets the requirements in all channels.

3.5. Detector characteristics

3.5.1. Dark frames, offsets, "first frame"

Dark frames for 200 second integrations for each channel are shown in Figure 5. Several hot pixels are seen in the images. Channels 1 and 2 show a minor "mux bleed" effect from the hot pixels, where a trail of pixels that are brighter than the image mean extends to the right of the hot pixels (in the readout direction). This elevated level is an offset that is stable and can be subtracted out and does not contribute to the noise. Section 3.5.3 below describes the mux bleed for pixels illuminated by a point source. In channels 3 and 4 a glow is seen in the lower right corner of the arrays due to emission from a FET off the edge of the array, and the top rows in the array exhibit higher background. The glow from the top rows is a result of the clocking scheme that was chosen to be robust against possible clamp gate failures that leaves the last row addressed during the integration. The glow in the lower right corner is at a level of about 20 e^-/sec, and makes these pixels noisier than ones in the dark regions of the image. However, the minimum in-flight background levels are expected to be 18 and 175 e^-/sec for channels 3 and 4 respectively, so the noise will be comparable or less than the noise from sky background.

The average pixel level in a dark is subject to a "first frame" effect where the first few frames in a series of back-to-back images have a different mean value than the remainder of the series. This is in part due to the fact that the arrays are reset every 200 ms if an integration is not currently underway. The reset strategy was adopted to prevent the arrays from saturating while waiting between integrations for the telescope to settle. The plot in Figure 6 shows the mean values of a series of five 30-sec frames in each channel. The exact curve is different for the various integration times, but similar. Five different series are plotted for each channel, taken on several different days. For each channel, the series is very repeatable – the ratio of the

Downloaded From: https://www.spiedigitallibrary.org/conference-proceedings-of-spie on 12/4/2018
Terms of Use: https://www.spiedigitallibrary.org/terms-of-use

first frames to the asymptotic value is stable from series to series. In a single time series, the large change is between the first and second image, the subsequent image means settle quickly to a stable value. The appearance of the first dark frame is slightly different from the subsequent frames in each channel, but the pattern in the image of each first frame is similar to other first frames. Taking a difference between two first frames shows no pattern difference above the noise, whereas the difference image between the first and second frame shows a pattern difference. In practice, most IRAC frames taken during the mission are likely to be first frames, since many observations will take only one image at each sky position, and there is a several second delay while the observatory points and settles to the new position.

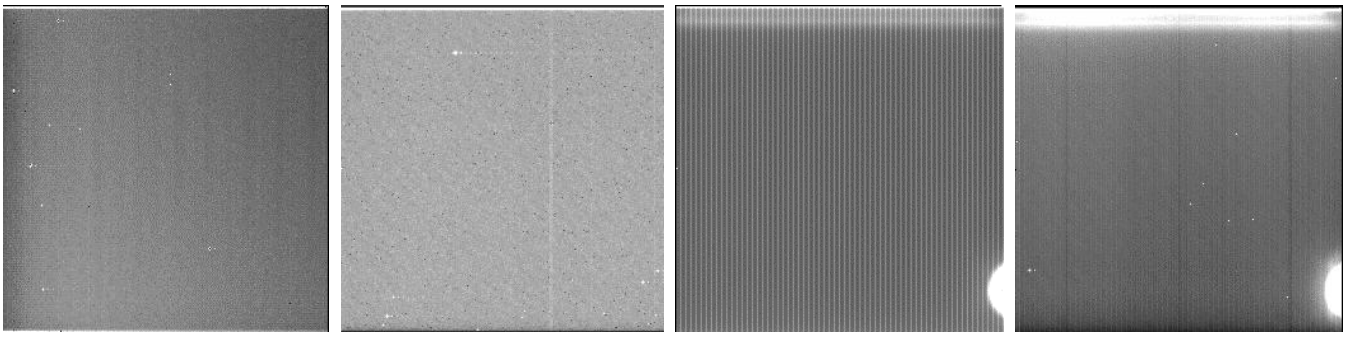

Figure 5. Dark frames (200 sec frame time) for channels 1 through 4.

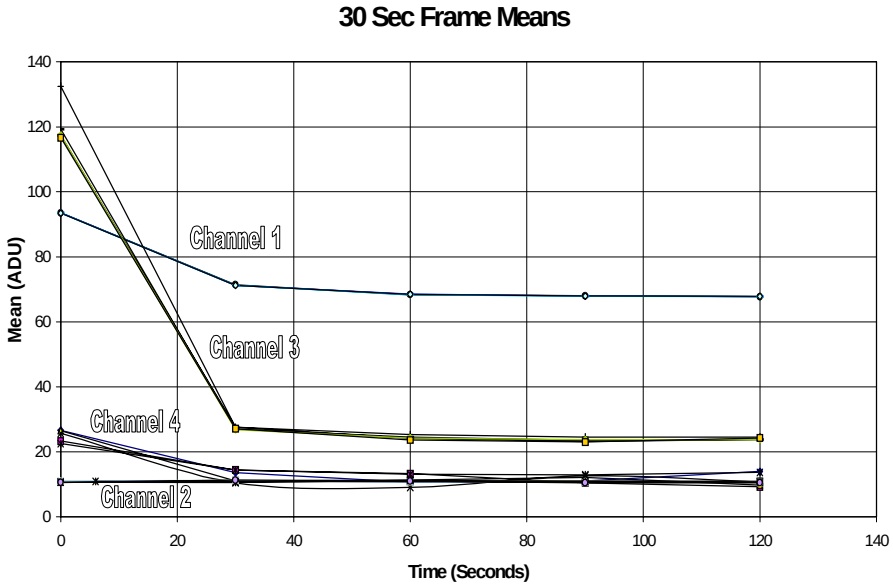

Figure 6. Image means of a series of 30 sec dark frames.

3.5.2. Residual images

The residual image performance of the arrays were tested on flight and flight-like parts at NASA/Ames[8] and University of Rochester[9]. Further work to characterize the flight arrays is ongoing at GSFC. One indicator of the residual performance is the relative level of the latent in the first frame following exposure to a bright source in a previous frame. For a exposure of 50,000 e^- fluence in 20 seconds, the residuals in the first frame following the exposure were measured to be 0.1, 0.05, 0.5, and 0.5 % of the previous fluence for channels 1-4, respectively.

Downloaded From: https://www.spiedigitallibrary.org/conference-proceedings-of-spie on 12/4/2018
Terms of Use: https://www.spiedigitallibrary.org/terms-of-use

3.5.3. Mux bleed in channels 1 and 2

The InSb arrays in channels 1 and 2 show a minor case of "mux bleed", where pixels in an output of the array following a bright source are higher than normal, and extend for much longer than expected given the bandwidth of the electronics. An example of this effect in channe1 1 is shown in Figure 7. There are two timescales, an initial quick decay with an intensity that varies non-linearly with the peak brightness, and an exponential decay whose intensity is proportional to the peak. The time constant of the decay is independent of the peak, at 48 pixel sample times (480 μsec). This effect will be corrected for in the pipeline data processing, so it is unlikely to affect the science data significantly.

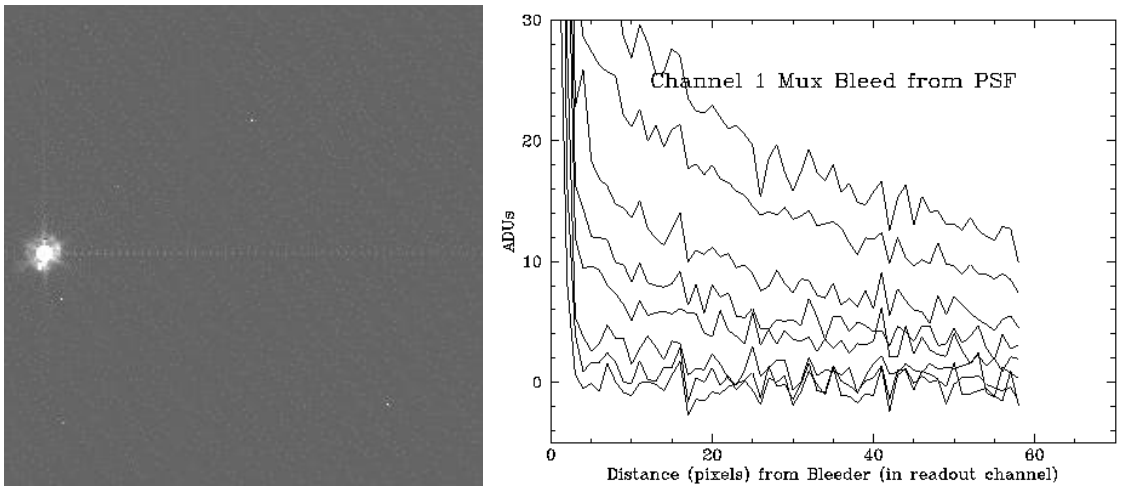

Figure 7. Mux bleed effect. The source in the channel 1 image on the left has a peak of 75,000 e^-, and the bleed can be seen trailing across the detector. The plot shows the mux bleed in one output channel (every 4th pixel) from sources with peaks of 4000, 20000, 40000, 55000, 75000, 95000, 111000, and 150000 e^-.

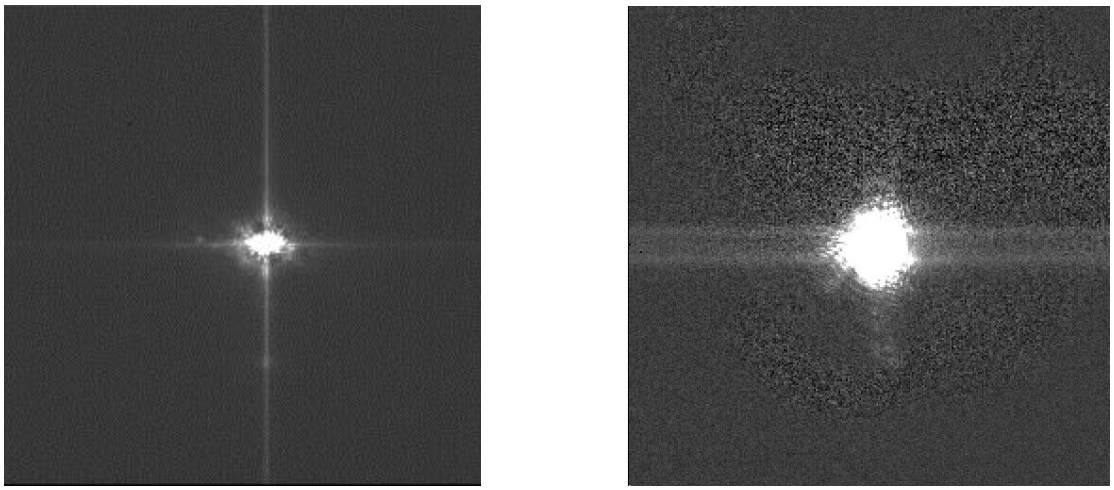

Figure 8. Banding in channel 3 (L) and channel 4 (R). The channel 4 image is of an out-of-focus "ring"; the faint bands extend from the brightest locations on the ring. The source peak signal value in channel 3 is about 1.6E+5 e^-, with a band of 120 e^- at 100 pixels from the peak. The values for channel 4 are 5.5E+4 and 500 e^- for the peak and the band, respectively.

3.5.4. Banding in channels 3 and 4

The Si:As arrays in channels 3 and 4 exhibit an effect known as "banding" or "streaking" with bright sources, where bands extend along the rows that contain a bright source. The effect is different that then mux bleed described above in that the intensity of the band does not fall off exponentially from the source but is roughly constant after ~10 pixels, it typically af-

Downloaded From: https://www.spiedigitallibrary.org/conference-proceedings-of-spie on 12/4/2018
Terms of Use: https://www.spiedigitallibrary.org/terms-of-use

fects all pixels in a row and several rows rather than a single output channel (therefore every 4th pixel in the image for mux bleed), and positive and/or negative bands can extend vertically along the columns of the peak pixels as well, as shown in Figure 8. The effect is stronger for channel 3 than channel 4, for point sources with comparable signal levels on the arrays. The magnitude of the effect has a non-linear correlation to the source intensity. We are currently working on algorithms to correct for this effect.

3.5.5. Crosstalk between channels

There are two kinds of crosstalk observed between the channels. One is that a bright point source in one channel will cause a faint apparent image or "ghost" in another channel that is not viewing the source. The effect was recently characterized using test point sources; the worst case was a source in channel 3 causing a ghost in channel 4 of 0.04% of the channel 3 intensity. The actual crosstalk levels experienced in-flight will probably depend on the performance of the flight cables.

A second effect is that performing a read on one detector will change the offset level of another detector. This can be seen in Figure 9, which shows the mean of images in channel 4 which is being read out every 50 seconds while the other frames are being read out every 200 seconds. Every time all four frames are read out, the mean is increased by a couple ADU. Then the following frame where only channel 4 is read out is much lower by about 10 ADU. For the second and third frames, the mean level is relatively constant.

This crosstalk effect is fairly benign and is very repeatable, therefore it can be corrected for in the data analysis and should not affect our ability to achieve the other calibration requirements. Whatever pixel read noise is contributed from crosstalk between channels is included in the measured value which is lower than the required maximum limit, so the added noise is not significant.

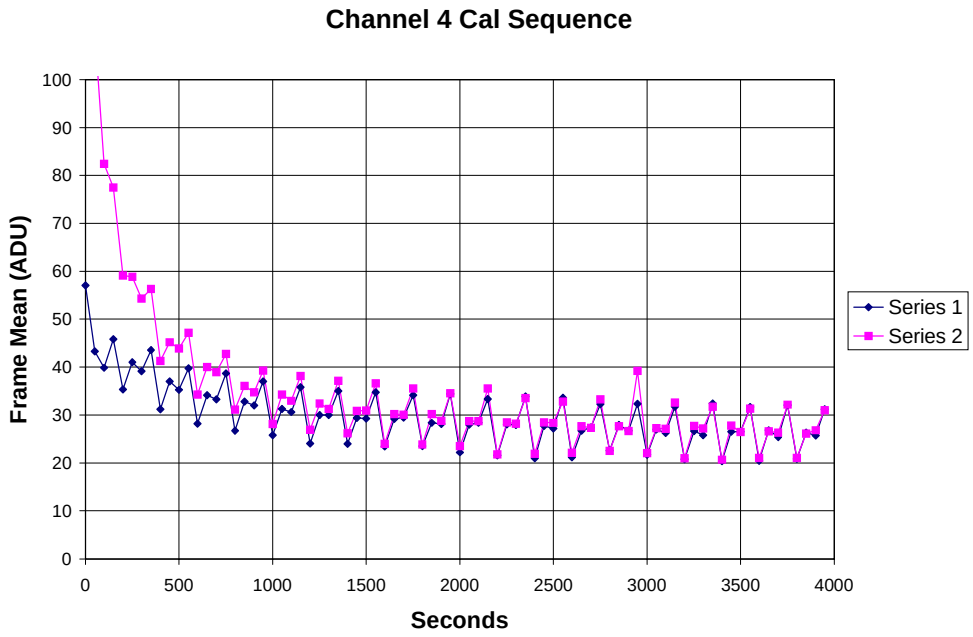

Figure 9. Channel 4 dark frame means.

3.5.6. Non-linearity

A linearization of the detectors was performed from the transmission calibration data. If we express the count level in a certain IRAC channel as S for integration time t, then (S/t) can be called the measured "signal rate", and

$$S/t = a \cdot S + b \quad (1)$$

Downloaded From: https://www.spiedigitallibrary.org/conference-proceedings-of-spie on 12/4/2018
Terms of Use: https://www.spiedigitallibrary.org/terms-of-use

should be a good first-order approximation of the non-linear behavior of the array (note that for a perfectly linear array response, the signal rate would be a constant, thus a = 0). We have used this formulation to fit the data, and the results are shown in Figure 10, where the fitting parameters (a, b) used are shown on the lower right hand side. One can see that the linear fit to the signal rate is indeed a reasonably good approximation of the data, up until the point near saturation where the signal rate rolls off sharply. In this representation, (1+a·S/b) becomes the factor by which one needs to correct the data for the measured fluxes.

The same fitting procedure as shown above in Figure 10 has been applied to the entire data frame and the fitting parameters a and b have been derived for every pixel. The numerical results (b/a) are presented here as image frames as well as histograms around the frame-wise mean value in Figure 11. It is seen that the pixel-to-pixel variation of parameter (b/a) is about 7% for the InSb arrays, and about 15% for the Si:As arrays. In obtaining these results we have limited the range of counts that enter the fitting to below about 35,000 ADU levels. The fact that the fitting of the (b/a) ratio is not a smoothly-varying function over the image frame in channel 4 is due to the over-exposure of the test (such that there were too few points below saturation to reach a stable fit). We have additional data that we will use for this channel to achieve a satisfactory fit. Finally, the full-frame fit also reveals some parts of the arrays that clearly have unusual gain factors, such as the horizontal linear feature in middle right of the channel 4 frame shown in Figure 11.

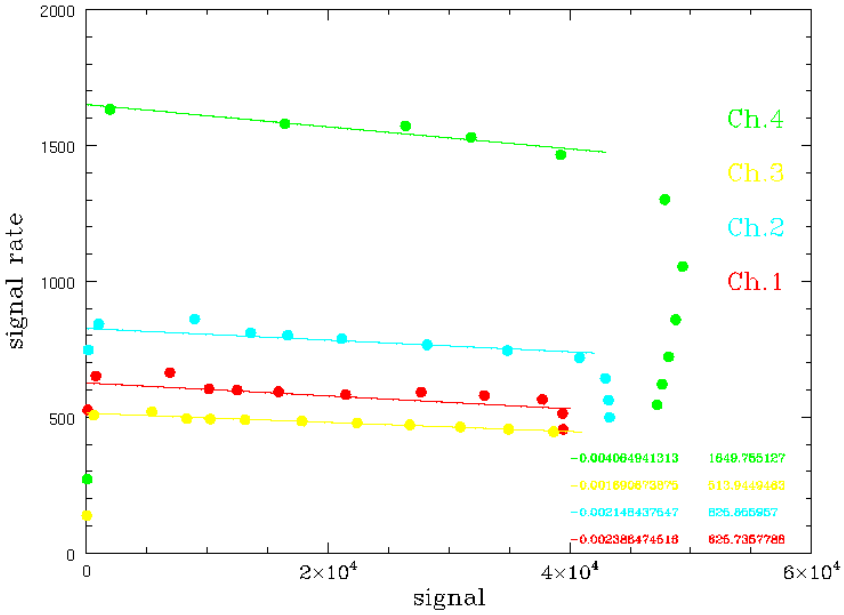

Figure 10. Signal rate vs. signal (counts): first-order fit for averaged signal. Signals are in ADUs.

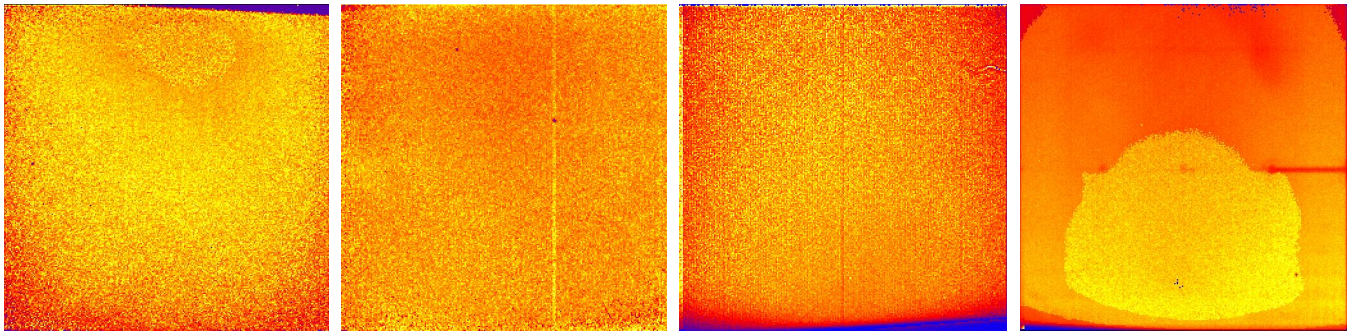

Figure 11. Non-linearity parameter "b/a": from first-order fit for entire arrays. Left to Right are channels 1 through 4.

Downloaded From: https://www.spiedigitallibrary.org/conference-proceedings-of-spie on 12/4/2018
Terms of Use: https://www.spiedigitallibrary.org/terms-of-use

4. SENSITIVITY ESTIMATE

The IRAC estimated point source sensitivity is given in Table 2. These are the point sources that would be detected at a 5 sigma level for the given frame times. The SIRTF top-level requirements for channel 1 and 4 point source sensitivity in these units are 3 and 28 μJy, respectively. The assumptions that went into this estimate are described below.

Table 2. IRAC 5 sigma point source sensitivities (μJy)

Frame Time (sec)	Channel 1	Channel 2	Channel 3	Channel 4
0.4	3905	4181	7128	3679
2	360	384	717	459
12	35	39.	105	105
30	14	18	52	63
100	5.1	7.7	24	33
200	3.1	5.0	16	23
500	1.8	3.1	10.1	14.5

4.1. Sensitivity Model

The Signal to Noise ratio (SNR) was calculated from the following equation:

$$\mathrm{SNRcalc}(t, F, BW, QE, I_d, r, N, \lambda) := \frac{F \cdot QE \cdot T_{Tel}(\lambda) \cdot T_{IRAC}(\lambda) \cdot A_T \cdot BW \cdot t \cdot \frac{1}{E_{ph}(\lambda)}}{\sqrt{QE \cdot T_{Tel}(\lambda) \cdot T_{IRAC}(\lambda) \cdot (F + N \cdot Bgnd(\lambda) \cdot 1.21 \cdot A_p) \cdot BW \cdot A_T \cdot t \cdot \frac{1}{E_{ph}(\lambda)} + N \cdot I_d \cdot t + N \cdot r^2}} \quad (2)$$

where

t = integration time in seconds
F = source flux in ergs/sec/cm^2/μm
BW = filter bandwidth (microns)
QE = Detector quantum efficiency
I_d = Dark current (electrons/sec)
r = read noise (electrons)
N = noise pixels
λ = wavelength of filter (microns)
T_{Tel} (λ)= telescope transmission
T_{IRAC} (λ) = IRAC optics transmission
E_{ph} (λ) = Energy (ergs) of a photon of wavelength λ
Bgnd(λ) = Cosmic background (ergs/sec/cm^2/sr/μm)
A_T = Telescope area (cm^2)
A_P = Pixel solid angle (sr)

4.2. Inputs to Model and Assumptions

Table 3 shows the inputs used in the sensitivity calculation. All values are measured except for the celestial background, telescope throughput and contamination degradation, noise pixels, and telescope area. The DQE values in the table are about 10% less than the measured values to give a conservative estimate of the sensitivity. The celestial background was estimated for the region at the ecliptic pole using an empirical model that is fitted to the COBE background measurements, excluding the contribution from stars that SIRTF will resolve. The factor of 1.21 applied to the celestial background is an estimate of

Downloaded From: https://www.spiedigitallibrary.org/conference-proceedings-of-spie on 12/4/2018
Terms of Use: https://www.spiedigitallibrary.org/terms-of-use

the straylight contribution of the SIRTF/IRAC system. The telescope throughput assumed is based on an estimate compiled by Ball Aerospace which includes measurements of the reflectivity of beryllium and an estimate of the effects of in-flight contamination levels on the optical surfaces. The calculation was performed for the central wavelength of each channel, assuming that all of the parameters are constant across the channel bandwidth including the spectral shape of the source. The noise pixel numbers were estimated by calculating the system PSF including expected aberrations in the SIRTF primary, jitter and drift during a 200 sec integration, and the effects of combining several dithered images to obtain an image.

Table 3. Model Inputs

Parameter	**Channel 1**	**Channel 2**	**Channel 3**	**Channel 4**
Central wavelength (microns)	3.5612	4.5095	5.6895	7.9584
Bandwidth (microns)	0.7500	1.015	1.435	2.930
Instrument optics throughput	0.689	0.744	0.569	0.540
Detector DQE	0.873	0.855	0.45	0.7
Detector dark current (e^-/sec)	0.1	0.28	1	3.8
Full Well (electrons)	150000	143500	190000	170000
Pixel size (arcsec)	1.2	1.2	1.2	1.2
Celestial background (ergs/cm^2/μm/sec/sr)	1.49	3.28	9.75	23.85
Celestial background (e^-/pixel/sec)	1.92	7.76	16.3	169
Telescope throughput	0.8886	0.9021	0.9081	0.9140
EOL contam. throughput degradation	0.0591	0.0591	0.077	0.077
Noise pixels	16	16	16	16
Telescope area (cm^2)	4636	4636	4636	4636

The read noises assumed in the sensitivity estimate are listed in Table 4. These are based on measurements of the read noise of the flight system during calibration tests performed in April 2000 at GSFC. Fowler sampling was used in all cases, where Fowler N sampling means that N array reads were taken at the start of the integration and N reads at the end, and the difference taken between the two sets of reads. There were several measurements at certain Fowler numbers for each of the channels. A median value of the measured noise was used rather than the best measured noise. Each number reported in the table is the full system noise, therefore the numbers include all sources including the internal noise of the flight electronics, noise from EMI, etc.

Table 4. Measured Read Noise

Frame time (sec)	0.4	2	12	30	100	200
Fowler number	1	4	8	16	16	32
Channel 1	28.3	15.3	12.3	10.8	10.8	8.2
Channel 2	34.9	18.7	13.9	13.3	13.3	8.7
Channel 3	26.3	15.0	14.8	14.5	14.5	13.0
Channel 4	29	16.6	12.6	10.8	10.8	9.9

5. ABSOLUTE CALIBRATION

5.1. Measurement of system sensitivity

The instrument absolute calibration was measured using a cryogenic blackbody in the test dewar at GSFC external to the IRAC instrument, positioned in front of the pickoff mirrors. A heater was used to set the blackbody to the desired temperature, and sensors on the blackbody surface gave the temperature at the time of the measurement. The blackbody was moved to several different offsets in the IRAC FOVs to allow correcting for any non-uniformity in the blackbody and to measure the throughput. The data were reduced as described in §3.3 above, and iteratively produced a consistent dark frame, flat field, and image of the blackbody source.

Downloaded From: https://www.spiedigitallibrary.org/conference-proceedings-of-spie on 12/4/2018
Terms of Use: https://www.spiedigitallibrary.org/terms-of-use

The results produced a calibration of the mean ADU/photon for each channel for photons incident on IRAC's pickoff mirror. The values obtained were within 10-20% of the expected values based on the component transmission and reflection measurements and the detector QEs. These tests were sufficient to show that IRAC is meeting its sensitivity requirements, but not to provide the required in-flight calibration. The throughput of the telescope and the actual surface contamination level will affect the absolute calibration as well, so the final calibration will have to use astronomical standards during the mission.

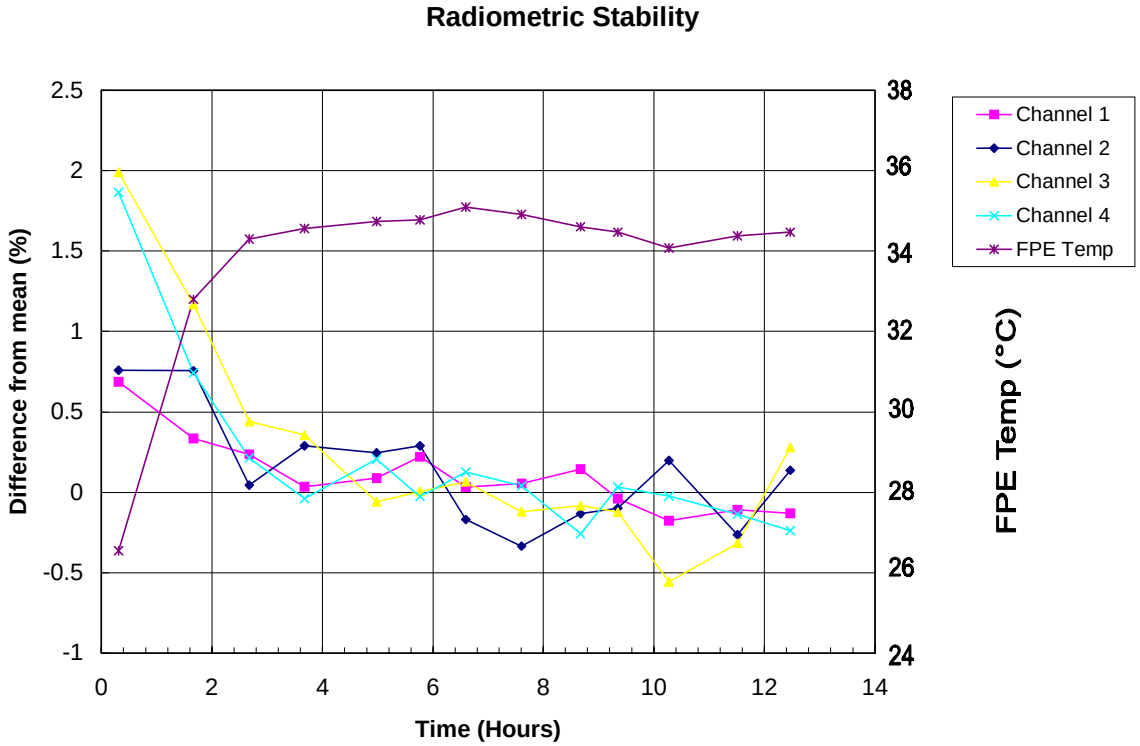

Figure 12. Stability of the transmission calibration sources. For each of the four channels, the % change from the mean measured calibration source intensity is plotted. Also shown is the temperature of the focal plane electronics (FPE) board during the test.

5.2. Instrument calibration subsystem stability

IRAC contains a transmission calibrator system which illuminates the detectors through the IRAC optics (excluding the pickoff mirror) by reflecting off a mirror on the back of the closed shutter. This can be used to track gain variations in the detectors, as well as the absolute responsivity of the system. The stability of the calibration lamps was measured during the calibration tests and is plotted in Figure 12. After the initial two hours after instrument turn-on, the system is stable to ±0.5% peak-to-peak. Changes in the measured calibration source intensity are due to either changes in the lamp intensity or in the detector system response. Measurements of astronomical standards will be used to track the system response to correct for any drift in the calibration system.

ACKNOWLEDGEMENTS

We acknowledge funding from NASA Office of Space Science for the work performed at the CfA and GSFC. We thank the Integration and Test group at GSFC for their excellent support of the IRAC testing program, including Ray Jungo, Ed Lander, Jim Golder, Juli Lander, Maureen Armbruster, Frank Carroll, Marty Brown, Michael Alexander, Ayman Mekhail, and Jim MacLeod.

Downloaded From: https://www.spiedigitallibrary.org/conference-proceedings-of-spie on 12/4/2018
Terms of Use: https://www.spiedigitallibrary.org/terms-of-use

REFERENCES

1. G. G. Fazio, J. L. Hora, S. P. Willner, J. R. Stauffer, M. L. N. Ashby, Z. Wang, E. V. Tollestrup, J. Pipher, W. Forrest, C. McCreight, S. H. Moseley, W. F. Hoffmann, P. Eisenhardt, & E. L. Wright, "The Infrared Array Camera (IRAC) for the Space Infrared Telescope Facility (SIRTF)", in *Infrared Astronomical Instrumentation*, ed. A. Fowler, Proc. SPIE 3354, pp. 1024-1031, 1998.
2. J. Wu, W. J. Forrest, J. L. Pipher, N. Lum, & A. Hoffman, "Development of infrared focal planes for space", Rev. Sci. Instrum., 68, pp. 3556-3578, 1997.
3. A. D. Estrada, G. Domingo, J. D. Garnett, A. W. Hoffman, N. A. Lum, P. J. Love, S. L. Solomon, J. E. Venzon, G. R. Chapman, K. D. Sparkman, C. McCreight, M. McKelvey, R. McMurray, J. Estrada, S. Zins, R. McHugh, & R. Johnson, "Si:As IBC IR Focal Plane Arrays for Ground-based and Space-based Astronomy", in *Infrared Astronomical Instrumentation,*ed. A. M. Fowler, Proc. SPIE 3354, pp. 99-108, 1998.
4. F. L. Selden et al., "Implementation and testing of SIRTF's Infrared Array Camera (IRAC)"in *Infrared Spaceborne Remote Sensing VIII*, eds. M. Stojnik & B. F. Andresen, Proc. SPIE, 4131, in press, 2000.
5. R. N. Hook & A. S. Fruchter, "Variable-pixel Linear Combination", in *Astronomical Data Analysis Software and Systems VI*, in A. S. P. Conf. Ser. vol. 125, eds. G. Hunt & H. E. Payne (San Francisco: ASP), p. 147, 1997.
6. K. P. Stewart & M. A. Quijada, "Cryo-transmittance and –reflectance of filters and beamsplitters for the SIRTF Infrared Array Camera", in *Infrared Spaceborne Remote Sensing VIII*, eds. M. Stojnik & B. F. Andresen, Proc. SPIE, 4131, in press, 2000
7. D. J. Fixsen, S. H. Moseley, & R. G. Arendt, "Calibrating Array Detectors", ApJSupp, 128, in press, 2000.
8. R. E. McMurray, Jr., R. R. Johnson, C. R. McCreight, M. E. McKelvey, J. D. Garnett, A. W. Hoffman, N. A. Lum, W. Y Lum, M. S. Smith, K. P. Sparkman, A. G. Toth, G. Domingo, D. J. Krebs, & M. D. Jhabvala, "Si:As IBC array performance for SIRTF/IRAC", in *Infrared Spaceborne Remote Sensing VIII*, eds. M. Stojnik & B. F. Andresen, Proc. SPIE, 4131, in press, 2000.
9. J. L. Pipher, W. J. Forrest, W. J. Glaccum, R. G. Benson, D. J. Krebs, M. D. Jhabvala, J.P. Rosbeck, N. A. Lum, W. Y. Lum, J. D. Garnett, A. W. Hoffman, & G. Domingo, "InSb arrays for IRAC (InfraRed Array Camera) on SIRTF (Space Infrared Telescope Facility)", in *Infrared Spaceborne Remote Sensing VIII*, eds. M. Stojnik & B. F. Andresen, Proc. SPIE, 4131, in press, 2000.

Downloaded From: https://www.spiedigitallibrary.org/conference-proceedings-of-spie on 12/4/2018
Terms of Use: https://www.spiedigitallibrary.org/terms-of-use